JCTC Journal of Chemical Theory and Computation

Article

pubs.acs.org/JCTC

Single Molecule Rectification Induced by the Asymmetry of a Single Frontier Orbital

Wendu Ding, Christian F. A. Negre,* Leslie Vogt, and Victor S. Batista*

Department of Chemistry, Yale University, P.O. Box 208107, New Haven, Connecticut 06520-8107, United States

Energy Sciences Institute, Yale University, P.O. Box 27394, West Haven, Connecticut 06516-7394, United States

Supporting Information

ABSTRACT: A mechanism for electronic rectification under low bias potentials is elucidated for the prototype molecule HS-phenyl-amide-phenyl-SH. We apply density functional theory (DFT) combined with the nonequilibrium Green's function formalism (NEGF), as implemented in the Tran-SIESTA computational code to calculate transport properties. We find that a single frontier orbital, the closest to the Fermi level, provides the dominant contribution to the overall transmission and determines the current. The asymmetric distribution of electron density in that orbital leads to rectification in charge transport due to its asymmetric response, shifting toward (or away from) the Fermi level under forward (or reverse) applied bias voltage. These findings provide a simple design principle to suppress recombination in molecular assemblies of dye-sensitized solar cells (DSSCs) where interfacial electron transfer is mediated by frontier orbitals with asymmetric character.

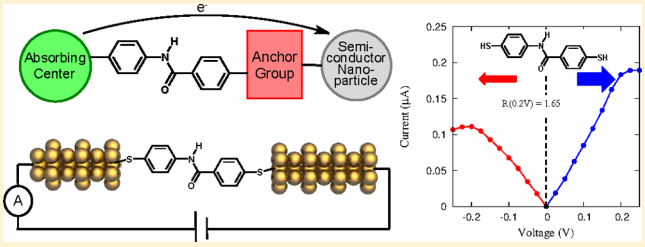

1. INTRODUCTION

Understanding charge transport in molecular assemblies of dye-sensitized solar cells (DSSCs) is a challenge of great interest since DSSCs could offer viable solutions to the renewable energy problem.[1−5] In such cells, the photoconversion mechanism is initiated by photoexcitation of dye molecules that are covalently bound to nanoporous semiconductor surfaces (e.g., TiO_2). The attachment is based on molecular linkers and anchoring groups, as schematically depicted in Figure 1. The photoexcited electrons are typically transferred through the molecular linkers and are then injected into the semiconductor matrix via ultrafast interfacial electron transfer (IET) dynamics.[5−12] To reduce back electron transfer, it would be desirable to have linkers with rectification properties, as indicated by the diode in Figure 1a, which would allow electrons to flow into the semiconductor but suppress recombination with the dye.[13,14] Here, we explore whether rectification at low bias voltages can be induced by amide groups conjugated to aromatic rings. We find that modest rectification (i.e., rectification ratio 1.4−1.6) is indeed feasible and that the underlying mechanism can be traced back to the asymmetry of a *single* state, the frontier orbital with maximum contribution to the overall transmission at the Fermi level. While the analysis is limited to the prototype molecule HS-phenyl-amide-phenyl-SH (A1), the mechanism should be common to other molecular assemblies with amide groups bridging the electron donor−acceptor fragments, such as sensitizers previously used in DSSCs[15] and porphyrin-fullerene dyads such as ZnP-NHCO-C_{60} and ZnP-CONH-C_{60} that have already been reported to exhibit different charge separation rates due to the switched order of the amide group.[16]

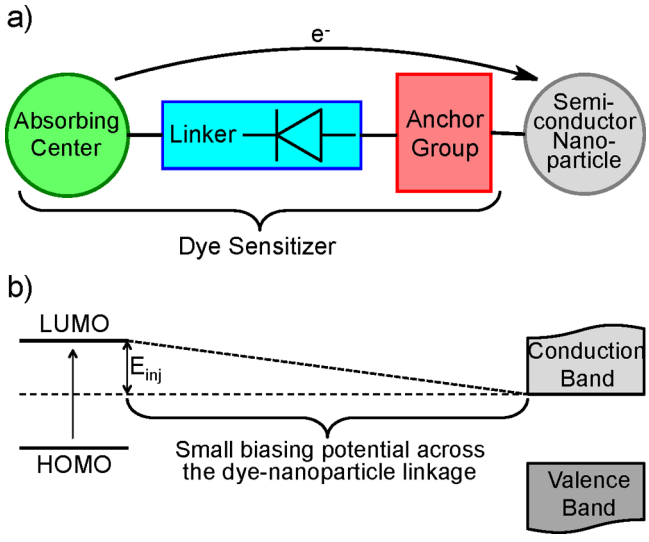

Figure 1. (a) Real-space representation of the components of an idealized DSSC. (b) Energetic scheme for the representation above with the energy difference between the dye LUMO and the conduction band creating the bias across the molecular linker.

Molecular rectifiers were first proposed by Aviram and Ratner more than 40 years ago.[17] Rectification has already been shown in self-assembled monolayers[18−23] where the surface field is important. However, single molecule rectification

Received: March 25, 2014
Published: July 15, 2014

   dx.doi.org/10.1021/ct5004687 | J. Chem. Theory Comput. 2014, 10, 3393−3400

remains to be demonstrated for molecules with rectification ratios >2.[24,25] In the limit of infinitesimal bias potentials, all molecules have symmetric current−voltage characteristics, regardless of their molecular symmetry, since the scattering transmission function is the same for electron tunneling forward or in reverse. Therefore, experimental studies and investigations based on the Landauer−Büttiker formalism[26,27] have focused on higher voltages. The outstanding challenge is to advance our understanding of rectification mechanisms at low bias potentials to develop design principles to guide the development of more effective molecular rectifiers. We focus on the study of rectification at low applied bias potentials since this regime is most relevant to DSSCs, where the voltage drop across molecular linkers is usually small (e.g., ≤ 250 mV). For example, in DSSCs based on the N3 dye, TiO_2 and I^-/I_3 electrolytes, the E_{inj} is about 200 mV.[5] In addition, depending on the distance from the absorbing center to the surface, the voltage gradient across the rectifying linker could be even smaller. While electron injection at higher voltages is possible, it is usually avoided, since it results in much lower efficiencies. This is a result of surface acceptor states being poised near the energetic edge of the conduction band and thus weakly coupled to donor states of much higher energy.[28] Therefore, rectifying linkers for DSSCs must exhibit satisfactory rectification at low bias voltages (i.e., early rectification). At these low bias voltages, molecular linkers are robust. Previous studies have reported successful single molecule conductance measurements with applied bias potentials of up to 1 V[25,29−31] and have shown that molecular structures can tolerate applied bias voltages of up to 5 V.[32]

We focus on the transport properties of the amide core in the prototype molecule HS-phenyl-amide-phenyl-SH, which is a synthetically accessible molecular linker previously used in DSSCs,[15] and in porphyrin-fullerene charge transfer dyads.[16] We analyze the nonequilibrium electronic properties of this molecular framework where the intrinsic asymmetry is introduced by the core amide group in an otherwise symmetric molecule. Our study is based on the analysis of transmission functions as a function of applied bias voltages, according to density functional theory (DFT) or a simple tight-binding model that provides valuable insights, calculations of $I-V$ curves computed by combining DFT and NEGF techniques,[33,34] and the inspection of the local density of states near the Fermi level.

A tight-binding model can provide a simple expression for the transmission, as a function of the applied bias voltage V, when a single state $|\varepsilon_0\rangle$ provides the dominant contribution to the current:

$$T(\varepsilon, V) = \frac{4\pi^2\gamma_L^2(V)\mathrm{DOS}_L(\varepsilon, V)\gamma_R^2(V)\mathrm{DOS}_R(\varepsilon, V)}{(\varepsilon - \varepsilon_0(V))^2 + \pi^2[\gamma_L^2(V)\mathrm{DOS}_L(\varepsilon, V) + \gamma_R^2(V)\mathrm{DOS}_R(\varepsilon, V)]^2} \quad (1)$$

where T is the transmission, ε_0 is the energy level of state $|\varepsilon_0\rangle$, $\gamma_{L/R}$ are the couplings between $|\varepsilon_0\rangle$ and the left (L) or right (R) leads, and DOS_L and DOS_R are the density of states for the two leads. A derivation of eq 1 is provided in the Supporting Information (SI). In the most general case, all of these functions $\gamma_{L/R}(V)$, $\mathrm{DOS}_{L/R}(\varepsilon,V)$, and $\varepsilon_0(V)$ depend on the applied voltage. While we do not use eq 1 for transport calculations, the tight-binding model is valuable, since it introduces the essential parameters that determine the different types of rectification mechanisms discussed below.

Rectification typically arises when $T(\varepsilon,V) \neq T(\varepsilon,-V)$ since the current is obtained by integrating the transmission function.[24] From eq 1, it is clear that the condition $T(\varepsilon,V) \neq T(\varepsilon,-V)$ can result from asymmetric couplings ($\gamma_L \neq \gamma_R$) under forward and reverse bias.[35−38] It can also result from contacts with different density of states (i.e., $\mathrm{DOS}_L \neq \mathrm{DOS}_R$)[39] or when $\varepsilon_0(V)$ shifts differently under positive and negative voltages. We focus on the shifting mechanism, which corresponds to *intrinsic rectification*, since it is determined by the *intrinsic electronic properties* of the molecule and it is observed even for symmetric couplings and an identical density of states for both leads.

Our analysis of transmission functions shows that conductance through HS-phenyl-amide-phenyl-SH is dominated by the transport properties of the HOMO, which is the state most proximal to the Fermi level. Due to the asymmetry of the amide group, the HOMO has an asymmetric distribution of charge preferentially localized on the aromatic ring that is more conjugated with the amide group. Such asymmetric charge distribution is stabilized (or destabilized) under positive (or negative) voltages inducing rectification. The underlying rectification is therefore quite different from other possible mechanisms, such as those based on pairs of donor−acceptor states in the molecule as proposed by Ratner and co-workers.[17] The mechanism that we observe also complements other studies of current rectification through $\pi\pi$ stacked multilayers,[40] rectification due to restructuring of frontier orbitals under strong bias voltage,[41−43] or rectification based on controlled molecular orientation as reported by Tao and co-workers.[29] Since it is observed under low bias voltages, it should be particularly valuable for the design of molecular linkers for DSSCs where asymmetric states near the Fermi level might dominate the IET dynamics.

2. STRUCTURAL MODELS AND METHODS

The molecular structures were built according to the usual three-system model, as shown in Figure 2, including the left electrode, central device molecular region, and the right electrode. The electrodes were modeled by using the Au (111) surface, as either thin nanowires built by repeating layers of 3 and 7 Au atom sublayers, or slabs built as semi-infinite 2D (111) fcc surfaces (see SI).[44−46] For the nanowires, each unit

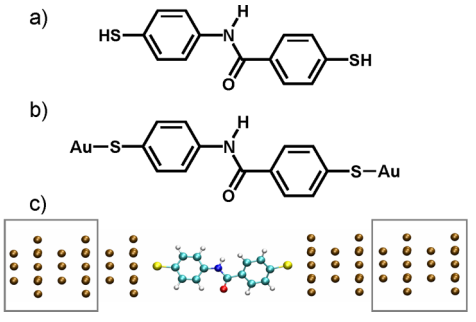

Figure 2. Schematic representation of 4-thio-N-(4-thiophenyl)-benzamide (HS-phenyl-amide-phenyl-HS) (a), 4-thio-N-(4-thiophenyl)benzamide bound to Au (Au-S-phenyl-amide-phenyl-S-Au) (b), and the Au-S-phenyl-amide-phenyl-S-Au system used to compute the transport properties using nanowire leads (c). The unit cells for the leads are indicated by boxes, while buffering Au layers connect the leads to the molecule. Color Key: Au, S, C, N, O, and H, are shown in golden, yellow, cyan, blue, red, and white spheres, respectively.

dx.doi.org/10.1021/ct5004687 | J. Chem. Theory Comput. 2014, 10, 3393−3400

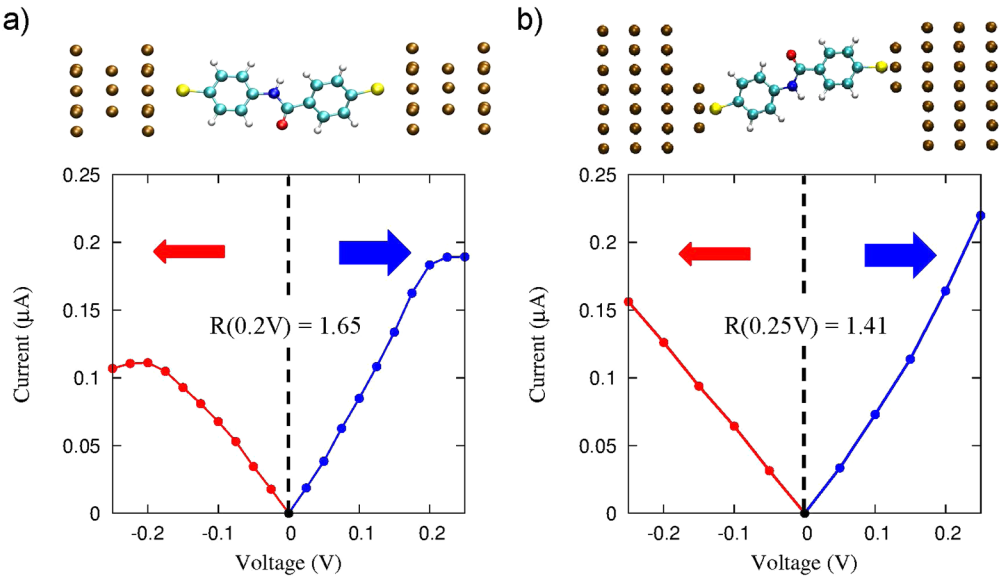

Figure 3. $I-V$ curves for Au_L-S-phenyl-amide-phenyl-S-Au_R show larger current values for positive applied bias than for negative applied bias. (a) Calculations performed with nanowire Au electrodes; (b) calculations performed with slab Au electrodes.

cell has two sublayers of seven and three atoms, respectively, that are repeated using periodic boundary conditions along the transport direction; each lead terminates in a seven atom face that mimics the Au (111) surface. The slab Au electrodes were modeled by using 6 layers of 16 gold atoms cut from an fcc lattice, with a single layer of a triad contact motif on the (111) surface to attach the molecule.[30,31] In either case, the Au (111) surface is used for attaching molecules because it is the most stable surface.[47] As discussed below, other Au surfaces might exhibit different values of absolute conductance and rectification ratios. However, the rectification mechanism should be insensitive to the nature of the lead since it is determined by the symmetry of molecular frontier orbitals. The molecule was connected to the gold electrodes via the thiolate anchoring groups. Transport properties were determined as usual by first describing the leads as semi-infinite periodic nanowires and subsequently connecting them to the central scattering region.

Molecular geometries for dithiol molecules were optimized at the DFT/B3LYP level[48] by using the 6-31G(d,p) basis set[49] as implemented in Gaussian 09 v.C01.[50] Starting from the optimized molecular coordinates for the HS-phenyl-amide-phenyl-SH system (Figure 2a), the extended molecule, Au_L-S-phenyl-amide-phenyl-S-Au_R (Figure 2c), was obtained by attaching the leads to compound -S-phenyl-amide-phenyl-S- without the two terminal H atoms. The Au−S distance was set to 2.32 Å, which corresponds to the DFT optimized bond length in Au-S-phenyl-amide-phenyl-S-Au (Figure 2b). Coordinates for the model systems are provided in the SI together with a sample input file for the transport calculations. We note that rectification trends are robust to changes in the Au−S bond-length (see SI). This is important for comparisons with break junction experiments that sample a distribution of Au−S distances and therefore a distribution of $I-V$ characteristics.[51]

Current−voltage characteristic curves were obtained by using the DFT-NEGF approach as implemented in the TranSIESTA computational package.[52] Even though the absolute values of conductance are systematically larger than the experimental data,[53] the trends in nonequilibrium transport properties predicted by DFT are fairly reliable.[25] Also, the self-consistent field (SCF) electron density redistribution that is critical for rectification is well captured by DFT.[54] A double-ζ basis set[55] was used for all transport calculations, which is sufficient to describe the dominant energy levels involved in electron transport. The generalized gradient approximation (GGA) functional PBE[56] was used as the exchange-correlation functional. We used different Monkhorst−Pack k-point grids to sample the Brillouin zone[57,58] for systems using the two types of gold electrodes. For the nanowire Au electrode, the k-point grid was $1 \times 1 \times 80$ for the leads and the gamma point for the molecular region; while for slab Au electrode, we used $10 \times 10 \times 80$ for the leads and $10 \times 10 \times 1$ for the molecular region. The energy cutoff for the real space grid was set to 200 Ry. The Hamiltonian matrix $H_{JK}^{\alpha\beta} = \langle \psi_J^{\alpha\beta} | H(\rho) | \psi_K^{\alpha\beta} \rangle$ was obtained from the DFT density matrix ρ, and the overlap matrix was $S_{JK}^{\alpha\beta} = \langle \psi_J^{\alpha\beta} | \psi_K^{\alpha\beta} \rangle$, where the indices J and K label the left (L) or right (R) leads, or the central (C) molecular region. Here, α and β represent orbital indices. These matrix elements are used to obtain the retarded Green's function of the central region $\mathcal{G}^+ = \frac{1}{\varepsilon S - H - \Sigma_L^+ - \Sigma_R^+}$, where an infinitesimal positive imaginary part has been added to the energy term. The $\Sigma_{L/R}^+$ functions are the self-energy terms of the left (L) and right (R) leads.

The density matrix $\rho = \frac{1}{2\pi i} \int \mathcal{G}_C^<(\varepsilon) d\varepsilon$ is defined in terms of the lesser Green's function $\mathcal{G}_C^<(\varepsilon)$ which is given by the nonequilibrium formalism as follows: $\mathcal{G}_C^<(\varepsilon) = i\mathcal{G}_C^+(\varepsilon)[\Gamma_L f(\varepsilon - \mu_L) + \Gamma_R f(\varepsilon - \mu_R)]\mathcal{G}_C^-(\varepsilon)$, with f the Fermi−Dirac distribution function and $\Gamma_{L/R} = i[\Sigma_{L/R}^+ - \Sigma_{L/R}^-]$.[31,59] Both the chemical potential of the electrodes $\mu_{L/R} = \varepsilon_F \pm V/2$ and the finite bias V are incorporated for the nonequilibrium regime and the electron density is calculated iteratively and self-consistently until convergence.

The transmission coefficient is obtained as usual, $T = \mathrm{Tr}[\Gamma_L \mathcal{G}_C^- \Gamma_R \mathcal{G}_C^+]$, while the current is obtained by integrating the transmission at 0 K, as follows:

dx.doi.org/10.1021/ct5004687 | J. Chem. Theory Comput. 2014, 10, 3393−3400

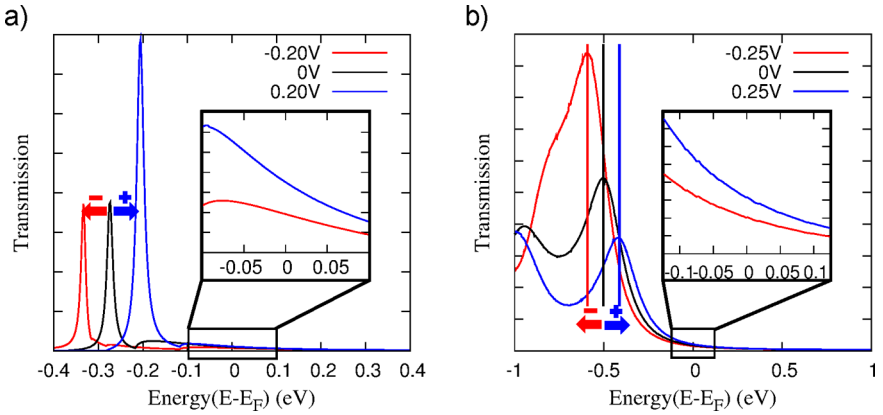

Figure 4. Transmission function for the molecular junction Au_L-S-phenyl-amide-phenyl-S-Au_R. (a) Calculations performed with nanowires Au electrodes. (b) Calculations performed with slab Au eletrodes. For panel a, the main peak is centered at −0.33, −0.28, and −0.20 eV for −0.20, 0.00, and +0.20 V bias, respectively. The insets show the transmission functions in the integration window from $-V/2$ to $+V/2$ used for the calculation of the currents at ±200 or 250 mV.

$$I(V) = \frac{2e}{h}\int_{-\infty}^{\infty} T(\varepsilon)[f(\varepsilon-\mu_L) - f(\varepsilon-\mu_R)]\mathrm{d}\varepsilon = \frac{2e}{h}\int_{\varepsilon_F-V/2}^{\varepsilon_F+V/2} T(\varepsilon)\mathrm{d}\varepsilon \quad (2)$$

The analysis of the origin of the asymmetry of the current−voltage characteristic curve is based on the response of the transmission function to positive and negative bias potentials as determined by the local density of states, which can also be obtained from Green's function as follows:[59,60]

$$\mathrm{LDOS}(\mathbf{r}, E) = -\frac{1}{\pi}\int_{E-\delta E}^{E+\delta E} \mathrm{Im}(\mathcal{G}^+(\mathbf{r}, \varepsilon))\mathrm{d}\varepsilon \quad (3)$$

where δE = 0.01 eV and E is the energy of interest. In this study, the LDOS is obtained by using the SIESTA computational package.[61] The local density of states LDOS(**r**,E) is particularly insightful since it provides a description of the distribution of charge density for a state of energy E, such as the HOMO that dominates electron transport in this prototype system.

3. RESULTS AND DISCUSSION

Figure 3 shows the I−V curve of Au-S-phenyl-amide-phenyl-S-Au calculated by using nanowire Au electrodes (Figure 3a) and slab Au electrodes (Figure 3b). The comparison provides insight on intrinsic rectification, which is observed for various types of leads, since it depends on molecular properties. Figure 3a clearly shows that the system exhibits modest rectification, with more current under positive bias than when a negative bias is applied. For the orientation shown in Figure 3, this corresponds to $\mu_L > \mu_R$, with electrons moving more easily from left to right. More generally, the electrons flow more readily from the nitrogen side to the carbonyl side of the molecule. The rectification ratio $R(V) = |I(+V)|/|I(-V)|$ is predicted to be 1.65 at 200 mV using the nanowire leads and 1.41 at 250 mV using the slab leads. We note that this magnitude of rectification is not predicted for other asymmetric molecules (see SI), making the phenyl-amide-phenyl system an intriguing case study.

To determine the origin of rectification in this prototype system, we analyze the transmission function (TF) without bias as compared to the corresponding transmission under positive and negative biasing potentials (Figure 4). We find that the main peak of the TF shifts toward the Fermi level (e.g., from −0.28 eV to −0.20 eV in Figure 4a) for a +200 mV applied bias (blue curve), but shifts in the opposite direction (e.g., from −0.28 eV to −0.33 eV in Figure 4a) for a −200 mV applied bias (red line). As a result, the I−V curve is asymmetric since the current computed as the area under the transmission function for the integration window from −100 mV to +100 mV (inset in Figure 4a) is larger for +200 mV than for −200 mV. The same effect is observed for calculations based on slab Au electrodes (as shown in Figure 4b), indicating that the underlying rectification mechanism is an intrinsic property of the molecule that is observed for different types of leads. It is noticeable that the width of the transmission functions are different when comparing results for the nanowire (panel a) or the slab electrodes (panel b). These widths are determined by the coupling strength and nanowires have fewer states (lower DOS near the Fermi level) that couple to the molecular HOMO (Figure S6 in SI). Hence, the transmission peaks for nanowire electrodes are narrower than those obtained for the slabs although they exhibit a similar response to the applied bias potentials.

To understand, at the molecular level, why the peak of the TF shifts in opposite directions when applying forward and reverse bias voltages, we analyze the distribution of charge density LDOS(**r**,E) at the corresponding energy E of the resonant state. Furthermore, we compute the projected density of states P-DOS for the left (S-phenyl-amide-) and right (-phenyl-S) parts of the molecular framework by simply summing over the atomic contributions of the corresponding molecular fragments (Figure 5a). This analysis shows that the state responsible for the resonance at −0.28 eV (indicated by the arrow in Figure 5a) is largely localized on the left side of the molecule (inset of Figure 5a). That state is thus *destabilized* and shifts toward the Fermi level (Figure 4) under forward bias since the potential is higher on the left and lower on the right (Figure 5b). Under reverse bias, the opposite effect is observed since the state is *stabilized* and therefore shifted away from the Fermi level (Figure 5b).

When comparing the electronic density of the transport channel at −0.28 eV to the density of the frontier orbitals of the isolated molecule (Figure 6), we find that the transport channel is very similar to the density of the HOMO, which is also asymmetrically localized on the left side of the molecule. In

dx.doi.org/10.1021/ct5004687 | J. Chem. Theory Comput. 2014, 10, 3393−3400

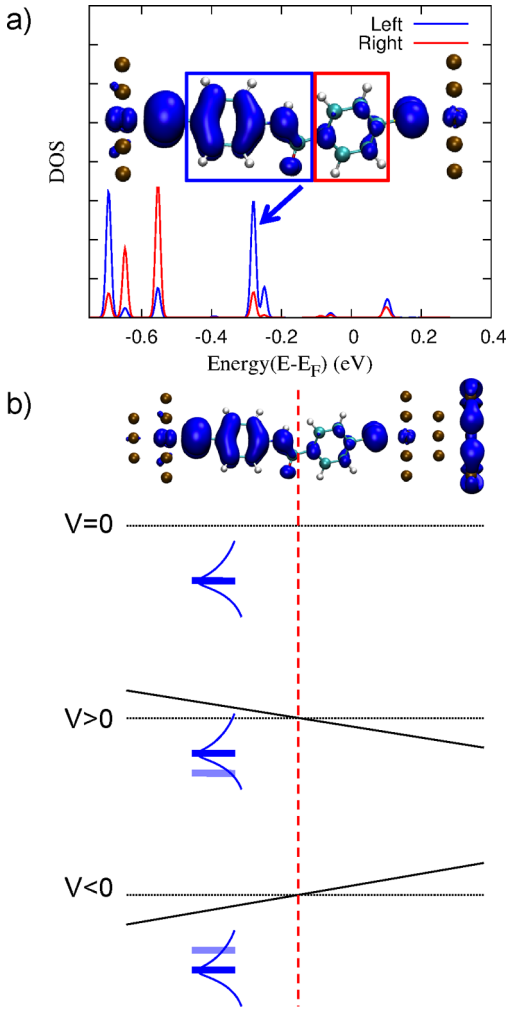

Figure 5. (a) Density of states (DOS) projected into the left (blue) and right (red) fragment of the molecular junction Au_L-S-phenyl-amide-phenyl-S-Au_R. The inset shows an isosurface of LDOS(**r**,*E*) for the transport channel state indicated by the arrow at $E = -0.28$ eV. (b) Shifting of the transport channel toward (or away from) the Femi level under the influence of forward (or reverse) bias potentials.

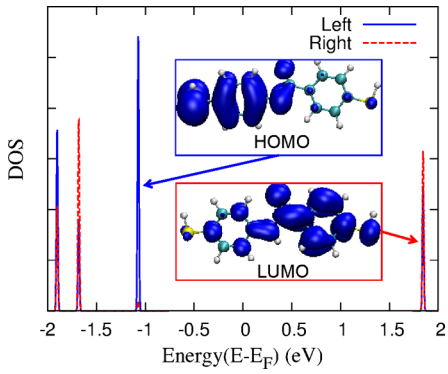

Figure 6. Density of states projected into the left (blue) and right (red) fragment of the isolated molecule HS-phenyl-amide-phenyl-SH. The inset shows an isosurface of LDOS(**r**,*E*) for the HOMO and LUMO states indicated by the blue and red arrows.

contrast, the LUMO is rather delocalized; it is therefore clear that the transport channel causing rectification is essentially the HOMO of the molecule, HS-phenyl-amide-phenyl-SH, mixed with electronic states of the leads, particularly in the case of the nanowire leads. Such electronic coupling poises the transport channel closer to the Fermi level.

To demonstrate the dramatic effect of the amide group on the symmetry of the transport channel responsible for the rectification properties of HS-phenyl-amide-phenyl-SH, Figure 7 shows the *I*−*V* curve and transmission functions after replacing the amide group by a carbon−carbon double bond. The resulting molecule (i.e., *trans*-stilbene, or molecule **A2**) is fully conjugated and planar. Figure 7 shows that the removal of the amide group symmetrizes the *I*−*V* curves and makes the response of the TF insensitive to the sign of the applied bias potential. This is simply due to the fact that the HOMO of the fully conjugated molecule has a symmetric distribution of charge density (Figure 8a). Figure 7 also shows that the extended conjugation increases the conductance when compared to the less conjugated molecule HS-phenyl-amide-phenyl-SH, in which the amide group introduces a 22° out-of-plane twist between the amide carbonyl group and the neighboring phenyl moiety. To show the importance of asymmetric transport channel localization, we have analyzed the transport properties of *trans*-stilbene after rotation of the right phenyl ring by 90° relative to the rest of the molecule, creating molecule **A3**. We believe that the rotation should induce rectification as it breaks the symmetric localization of transport channel. Figure 8b shows that such conformational change breaks the extended conjugation and localizes the electron density on the left side of the molecule (i.e., on the S-phenyl-C═C- fragment). As anticipated, the resulting conformationally constrained system exhibits significant rectification (e.g., a rectification ratio of 1.51 at 200 mV, as shown in Figure 9, comparable to the rectification ratio of the molecule with the amide group), although with much lower conductance due to the broken conjugation. The design of molecular frameworks with rectification properties could thus focus on substitutional groups that would stabilize such conformations to induce localization of the transport channel on one side of the molecular junction, either due to chemical modification via functionalization or conformational changes.

4. CONCLUSIONS

We have found a mechanism for rectification of electron transport in the prototype molecule HS-phenyl-amide-phenyl-SH that is determined by the asymmetric distribution of charge in the frontier orbital most proximal to the Fermi level. An asymmetrically localized transport channel provides the dominant contribution to the transmission function in the integration energy window used for calculations of the current as a function of voltage, and this state responds by shifting toward (or away from) the Fermi level under forward (or reverse) applied bias voltages.

Contrary to mechanisms based on donor−acceptor dyads where both donor and acceptor states in the molecule participate in the transport mechanism, the rectification properties of Au-S-phenyl-amide-phenyl-S-Au are determined by the asymmetric distribution of charge in the HOMO due to the amide group, giving the resulting stabilization (or destabilization), relative to the Fermi level, under the influence of negative (or positive) potentials. This mechanism complements other possible rectification schemes, such as those based on donor−acceptor dyads,[17] or controlled molecular orientation.[29] At the same time, the reported results suggest a simple principle for design of molecular rectifiers where electron

dx.doi.org/10.1021/ct5004687 | J. Chem. Theory Comput. 2014, 10, 3393−3400

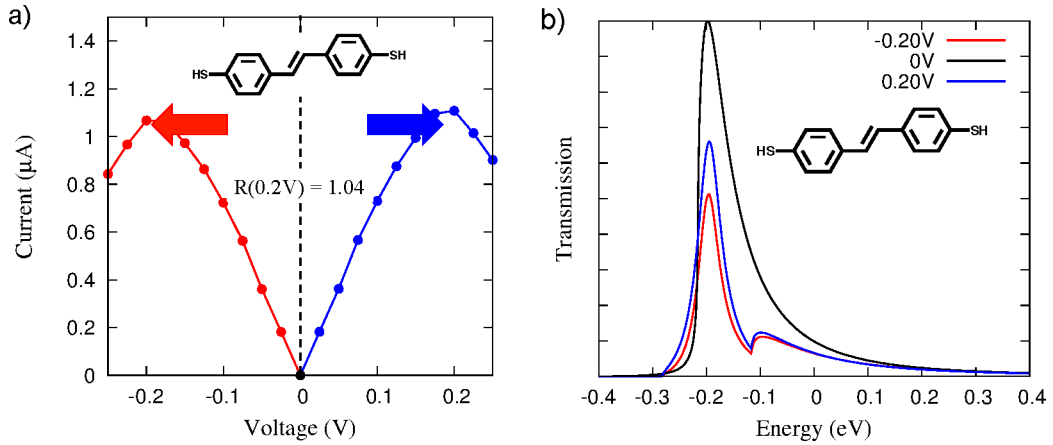

Figure 7. (a) $I-V$ curve for Au_L-S-stilbene-S-Au_R showing no rectification. (b) Transmission functions for Au_L-S-stilbene-S-Au_R at zero and ±200 mV.

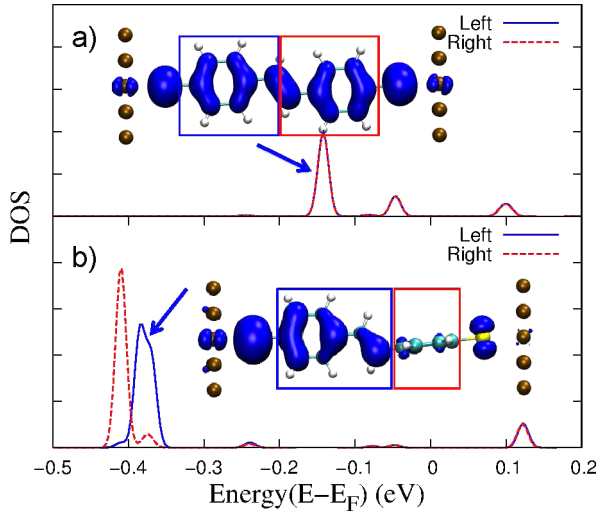

Figure 8. Density of states (DOS) projected into the left (blue) and right (red) fragment of the molecular junction Au_L-S-phenyl-C≡C-phenyl-S-Au_R in its minimum energy coplanar configuration (a) and after out-of-plane rotation of the right phenyl ring by 90° (b). The insets show the isosurfaces of LDOS(**r**,E) for the transport channel state indicated by the arrows.

transport is mediated by a single frontier orbital channel (e.g., the HOMO or the LUMO) with an asymmetric distribution of charge density along the transport direction. Such molecular components should be particularly valuable in applications to dye-sensitized solar cells (DSSCs) or organic photovoltaic devices where the overall efficiency is often affected by detrimental recombination processes.

■ ASSOCIATED CONTENT

Ⓢ Supporting Information

Derivation of **1**, $I-V$ curves for bis-phenyl amide with S–Au distance dependence and molecule rotation dependence, coordinates for structures of bis-phenyl amide and E-stilbene, sample input file for TranSIESTA calculation. This material is available free of charge via the Internet at http://pubs.acs.org/.

■ AUTHOR INFORMATION

Corresponding Authors

*Email: christian.negre@yale.edu.
*Email: victor.batista@yale.edu.

Notes

The authors declare no competing financial interest.

■ ACKNOWLEDGMENTS

We acknowledge support by the Office of Basic Energy Sciences of the U.S. Department of Energy (DE-FG02-07ER15909) for the analysis of molecular rectifiers and supercomputer time from NERSC, XSEDE, and the Yale

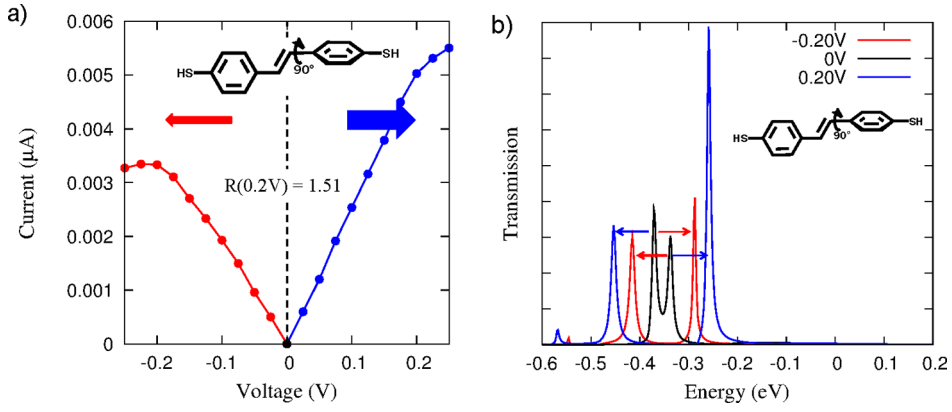

Figure 9. (a) $I-V$ curve for Au_L-S-stilbene-S-Au_R with 90° twist angle showing larger current values for positive applied voltage than for negative applied voltages. (b) Transmission function for Au_L-S-stilbene-S-Au_R with 90° twist angle.

University Faculty of Arts and Sciences High Performance Computing Center partially funded by the National Science Foundation grant CNS 08-21132. The work on methods development was supported as part of the Argonne-Northwestern Solar Energy Research (ANSER) Center, an Energy Frontier Research Center funded by the U.S. Department of Energy, Office of Science, Office of Basic Energy Sciences under Award Number DE-SC0001059. We thank Prof. A. R. Rocha and R. Amorim for helpful discussions.

REFERENCES

(1) Abuabara, S. G.; Cady, C. W.; Baxter, J. B.; Schmuttenmaer, C. A.; Crabtree, R. H.; Brudvig, G. W.; Batista, V. S. *J. Phys. Chem. C* **2007**, *111*, 11982−11990.
(2) Balzani, V.; Credi, A.; Venturi, M. *ChemSusChem* **2008**, *1*, 26−58.
(3) McConnell, I.; Li, G.; Brudvig, G. W. *Chem. Biol.* **2010**, *17*, 434−447.
(4) Cady, C. W.; Crabtree, R. H.; Brudvig, G. W. *Coord. Chem. Rev.* **2008**, *252*, 444−455.
(5) Hagfeldt, A.; Boschloo, G.; Sun, L.; Kloo, L.; Pettersson, H. *Chem. Rev.* **2010**, *110*, 6595−6663.
(6) Rego, L. G. C.; Batista, V. S. *J. Am. Chem. Soc.* **2003**, *125*, 7989−7997.
(7) Negre, C. F. A.; Milot, R. L.; Martini, L. A.; Ding, W.; Crabtree, R. H.; Schmuttenmaer, C. A.; Batista, V. S. *J. Phys. Chem. C* **2013**, *117*, 24462−24470.
(8) Brewster, T. P.; Konezny, S. J.; Sheehan, S. W.; Martini, L. A.; Schmuttenmaer, C. A.; Batista, V. S.; Crabtree, R. H. *Inorg. Chem.* **2013**, *52*, 6752−6764.
(9) Young, K. J.; Martini, L. A.; Milot, R. L.; Snoeberger, R. C., III; Batista, V. S.; Schmuttenmaer, C. A.; Crabtree, R. H.; Brudvig, G. W. *Coord. Chem. Rev.* **2012**, *256*, 2503−2520.
(10) Moore, G. F.; Konezny, S. J.; Song, H.-e.; Milot, R. L.; Blakemore, J. D.; Lee, M. L.; Batista, V. S.; Schmuttenmaer, C. A.; Crabtree, R. H.; Brudvig, G. W. *J. Phys. Chem. C* **2012**, *116*, 4892−4902.
(11) McNamara, W. R.; Milot, R. L.; Song, H.-e.; Snoeberger, R. C., III; Batista, V. S.; Schmuttenmaer, C. A.; Brudvig, G. W.; Crabtree, R. H. *Energy Env. Sci.* **2010**, *3*, 917−923.
(12) Li, G.; Richter, C. P.; Milot, R. L.; Cai, L.; Schmuttenmaer, C. A.; Crabtree, R. H.; Brudvig, G. W.; Batista, V. S. *Dalton Trans.* **2009**, 10078−10085.
(13) Senevirathna, M. K. I.; Pitigala, P. K. D. D. P.; Perera, V. P. S.; Tennakone, K. *Langmuir* **2005**, *21*, 2997−3001.
(14) Ding, W.; Negre, C. F. A.; Palma, J. L.; Durrell, A. C.; Allen, L. J.; Young, K. J.; Milot, R. L.; Schmuttenmaer, C. A.; Brudvig, G. W.; Crabtree, R. H.; Batista, V. S. *ChemPhysChem* **2014**, *15*, 1138−1147.
(15) McNamara, W. R.; Snoeberger, R. C.; Li, G.; Schleicher, J. M., III; Cady, C. W.; Poyatos, M.; Schmuttenmaer, C. A.; Crabtree, R. H.; Brudvig, G. W.; Batista, V. S. *J. Am. Chem. Soc.* **2008**, *130*, 14329−14338.
(16) Imahori, H.; Yamada, H.; Guldi, D.; Endo, Y.; Shimomura, A.; Kundu, S.; Yamada, K.; Okada, T.; Sakata, Y.; Fukuzumi, S. *Angew. Chem., Int. Ed.* **2002**, *41*, 2344−2347.
(17) Aviram, A.; Ratner, M. *Chem. Phys. Lett.* **1974**, *29*, 277−283.
(18) Reinerth, W. A.; Jones, L., II; Burgin, T. P.; w Zhou, C.; Muller, C. J.; Deshpande, M. R.; Reed, M. A.; Tour, J. M. *Nanotechnology* **1998**, *9*, 246.
(19) Chen, J.; Reed, M. A.; Rawlett, A. M.; Tour, J. M. *Science* **1999**, *286*, 1550−1552.
(20) Chen, J.; Reed, M. A. *Chem. Phys.* **2002**, *281*, 127−145.
(21) Petty, M., Bryce, M. R., Bloor, D., Eds. *An Introduction to Molecular Electronics*; Oxford University Press: New York, 1995.
(22) Metzger, R. M.; Chen, B.; Höpfner, U.; Lakshmikantham, M. V.; Vuillaume, D.; Kawai, T.; Wu, X.; Tachibana, H.; Hughes, T. V.; Sakurai, H.; Baldwin, J. W.; Hosch, C.; Cava, M. P.; Brehmer, L.; Ashwell, G. J. *J. Am. Chem. Soc.* **1997**, *119*, 10455−10466.
(23) Nijhuis, C. A.; Reus, W. F.; Whitesides, G. M. *J. Am. Chem. Soc.* **2010**, *132*, 18386−18401.
(24) Mujica, V.; Ratner, M. A.; Nitzan, A. *Chem. Phys.* **2002**, *281*, 147−150.
(25) Batra, A.; Darancet, P.; Chen, Q.; Meisner, J. S.; Widawsky, J. R.; Neaton, J. B.; Nuckolls, C.; Venkataraman, L. *Nano Lett.* **2013**, *13*, 6233−6237.
(26) Landauer, R. *Philos. Mag.* **1970**, *21*, 863−867.
(27) Büttiker, M. *Phys. Rev. Lett.* **1986**, *57*, 1761−1764.
(28) Fuertes, V. C.; Negre, C. F. A.; Oviedo, M. B.; Bonafé, F. P.; Oliva, F. Y.; Sánchez, C. G. *J. Phys.: Condens. Matter* **2013**, *25*, 115304.
(29) Diez-Perez, I.; Hihath, J.; Lee, Y.; Yu, L.; Adamska, L.; Kozhushner, M. A.; Oleynik, I. I.; Tao, N. *Nat. Chem.* **2009**, *1*, 635−641.
(30) Quek, S. Y.; Venkataraman, L.; Choi, H. J.; Louie, S. G.; Hybertsen, M. S.; Neaton, J. B. *Nano Lett.* **2007**, *7*, 3477−82.
(31) Darancet, P.; Widawsky, J.; Choi, H.; Venkataraman, L.; Neaton, J. *Nano Lett.* **2012**, *12*, 6250−6254.
(32) Di Ventra, M.; Pantelides, S. T.; Lang, N. D. *Phys. Rev. Lett.* **2002**, *88*, 046801.
(33) Keldysh, L. V. *Sov. Phys. JETP* **1965**, *20*, 1018−1026.
(34) Datta, S., Ed. *Quantum Transport*; Cambridge University Press: Cambridge, U.K., 2005.
(35) Ford, M. J.; Hoft, R. C.; McDonagh, A. M.; Cortie, M. B. *J. Phys.: Condens. Matter* **2008**, *20*, 374106.
(36) Zhang, Z.; Yang, Z.; Yuan, J.; Qiu, M. *J. Chem. Phys.* 2008, *128*.
(37) Zhao, J.; Yu, C.; Wang, N.; Liu, H. *J. Phys. Chem. C* **2010**, *114*, 4135−4141.
(38) Martin, S.; Manrique, D. Z.; García-Surez, V. M.; Haiss, W.; Higgins, S. J.; Lambert, C. J.; Nichols, R. J. *Nanotechnology* **2009**, *20*, 125203.
(39) Pan, J. B.; Zhang, Z. H.; Ding, K. H.; Deng, X. Q.; Guo, C. *Appl. Phys. Lett.* **2011**, *98*, 013503.
(40) Tsuji, Y.; Yoshizawa, K. *J. Phys. Chem. C* **2012**, *116*, 26625−26635.
(41) Staykov, A.; Nozaki, D.; Yoshizawa, K. *J. Phys. Chem. C* **2007**, *111*, 11699−11705.
(42) Pan, J. B.; Zhang, Z. H.; Deng, X. Q.; Qiu, M.; Guo, C. *Appl. Phys. Lett.* **2010**, *97*, 203104.
(43) Staykov, A.; Li, X.; Tsuji, Y.; Yoshizawa, K. *J. Phys. Chem. C* **2012**, *116*, 18451−18459.
(44) Krstić, P. S.; Zhang, X.-G.; Butler, W. H. *Phys. Rev. B* **2002**, *66*, 205319.
(45) Zhang, X.-G.; Krstić, P. S.; Butler, W. H. *Int. J. Quantum Chem.* **2003**, *95*, 394−403.
(46) Krstić, P. S.; Dean, D. J.; Zhang, X.-G.; Keffer, D.; Leng, Y. S.; Cummings, P. T.; Wells, J. C. *Comput. Mater. Sci.* **2003**, *28*, 321−341.
(47) Rodrigues, V.; Fuhrer, T.; Ugarte, D. *Phys. Rev. Lett.* **2000**, *85*, 4124−4127.
(48) Lee, C.; Yang, W.; Parr, R. G. *Phys. Rev. B* **1988**, *37*, 785−789.
(49) Hehre, W. J.; Radom, L.; Schleyer, P. v. R.; Pople, J. A. *Ab Initio Molecular Orbital Theory*; Wiley: New York, 1986.
(50) Frisch, M. J.; Trucks, G. W.; Schlegel, H. B.; Scuseria, G. E.; Robb, M. A.; Cheeseman, J. R.; Scalmani, G.; Barone, V.; Mennucci, B.; Petersson, G. A.; et al.; *Gaussian 09*, Revision C.01; Gaussian Inc.: Wallingford, CT, 2009.
(51) Hoft, R. C.; Ford, M. J.; Garciía-Suaárez, V. M.; Lambert, C. J.; Cortie, M. B. *J. Phys.: Condens. Matter* **2008**, *20*, 025207 .
(52) Brandbyge, M.; Mozos, J. L.; Ordejón, P.; Taylor, J.; Stokbro, K. *Phys. Rev. B* **2002**, *65*, 165401.
(53) Ding, W.; Negre, C. F. A.; Vogt, L.; Batista, V. S. *J. Phys. Chem. C* **2014**, *118*, 8316−8321.
(54) Negre, C. F. A.; Gallay, P. A.; Sánchez, C. G. *Chem. Phys. Lett.* **2008**, *460*, 220−224.
(55) Junquera, J.; Paz, O.; Sánchez-Portal, D.; Artacho, E. *Phys. Rev. B* **2001**, *64*, 235111.
(56) Perdew, J. P.; Burke, K.; Ernzerhof, M. *Phys. Rev. Lett.* **1996**, *77*, 3865−3868.
(57) Monkhorst, H. J.; Pack, J. D. *Phys. Rev. B* **1976**, *13*, 5188−5192.

(58) Pack, J. D.; Monkhorst, H. J. *Phys. Rev. B* **1977**, *16*, 1748−1749.
(59) Zahid, F.; Paulsson, M.; Datta, S. Electrical Conduction through Molecules. In *Advanced Semiconductor and Organic Nano-Techniques III: Physics and Technology of Molecular and Biotechnology Systems*; Morkoç, H., Ed.; Academic Press: San Diego, 2003; Chapter 1, pp 1 − 41.
(60) Economou, E. *Green's Functions in Quantum Physics*, 3rd ed.; Springer Series in Solid-State Sciences; Springer: New York, 2006.
(61) Soler, J. M.; Artacho, E.; Gale, J. D.; García, A.; Junquera, J.; Ordejón, P.; Sánchez-Portal, D. *J. Phys.: Condens. Matter* **2002**, *14*, 2745−2779.